Proceedings of ASME Turbo Expo 2011
GT2011
June 6-10, 2011, Vancouver, British Columbia, Canada

GT2011-45342

DESIGN AND TEST OF A HIGHLY LOADED SINGLE-STAGE HIGH PRESSURE TURBINE

T. Wolf
Rolls-Royce Deutschland
Dahlewitz, Germany

E. Janke
Rolls-Royce plc
Derby, United-Kingdom

R. Benton
Rolls-Royce Deutschland
Dahlewitz, Germany

F. Kost
DLR
Göttingen, Germany

F. Haselbach
Rolls-Royce plc
Derby, United Kingdom

S. Gegg
Rolls-Royce Corporation
Indianapolis, IN, United States

ABSTRACT

For the small to medium thrust range of modern aero engines, highly loaded single-stage HP turbines facilitate an attractive alternative to a more conventional 2-stage HPT architecture. Within the German government funded LUFO-3 programme "Transonic Single Stage High-Pressure Turbine", a substantial activity towards the development and test of supersonic aerodynamic technology for single stage turbines was launched in 2003. This paper describes fundamental aerodynamic concept studies and related cascade experiments in support of a future highly loaded high-pressure turbine architecture. Details of the first out of two builds featuring an engine representative single-stage HPT is described in detail. Focus will be on instrumentation design, selected results from performance, area traverse and unsteady blade surface pressure measurements and the comparison of experiments with numerical simulations. The successfully completed test campaign confirms the existence of an aerodynamically efficient design of a highly loaded HPT, thereby enabling a competitive building block for a small to medium size engine concept.

NOMENCLATURE

α	[°]	flow angle
c_p	[J/kg]	specific heat at constant pressure
DHT	[J/kg K]	rotor specific work
η	[-]	efficiency
Ma	[-]	Mach number
N	[min^{-1}]	rotational speed
NHRT	[$\text{min}^{-1}/\sqrt{\text{K}}$]	reduced speed
φ	[°]	circumferential coordinate
p	[Pa]	pressure
P	[W]	Power
PR	[-]	pressure ratio
R	[J/kg/K]	gas constant
T	[K]	temperature
w	[kg/s]	mass flow
WRTP	[kg $\sqrt{\text{K}}$ /kPa]	capacity
40		stator inlet plane
41		stator exit plane
44		exit duct
is		isentropic
r		rotor
t		total quantity
HPT		High Pressure Turbine
HWSS		High-Work Single-Stage HPT

INTRODUCTION

The increasing pressure to reduce emissions and fuel consumption forces aircraft engine manufacturers to continuously enhance their products. Additional aims are the reduction of complexity and thus cost as well as size and weight. In the small to medium thrust aero engine an attractive way to meet these requirements is to move from a conventional two-stage HPT design to a highly-loaded single-stage concept running at higher, i.e., supersonic exit Mach numbers. The targeted operating point of such a design compared to conventional HPTs is illustrated in Figure 1. While the latter run at expansion ratios of >2, a change towards higher pressure

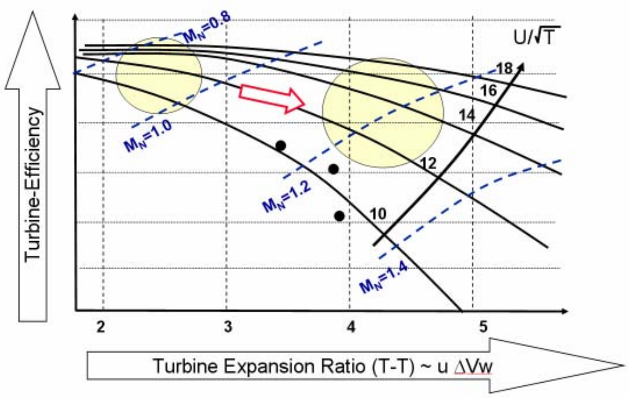

Figure 1: Targeted operating point of transonic HPT

ratios and at the same time competitive efficiencies requires an increase of reduced speed $N/\sqrt{T}$ and thus a higher rotational speed and lower HP inlet temperature. The advantages of such a modern design are a shorter turbine length and reduced component cost and possibly weight as well, whereas efficiency penalties due to the higher velocity cannot be avoided. The design space for a highly loaded HPT is bound by several physical barriers. A desirable operating point should lie outside of the transonic regime, which is usually associated with unsteadiness and inherent flow instability whereas for increasing Mach numbers shock induced losses become dominating. In order to maintain a given specific work the two main parameters rotational speed and blade loading need to be chosen carefully, as increasing stresses especially in the disc and blade-disc interface demand costly materials or sturdier designs while on the aerodynamic side the flow becomes prone to separation. It is the aerodynamicist's task to design a supersonic turbine aerofoil such that an optimal loss behaviour within the given limits of material choice and available space is achieved, and the resulting engine is economically more attractive than a conventional design.

The potential of transonic and supersonic turbine aerofoils has been investigated experimentally since the mid 1970s at VKI, the first works focusing on aerodynamic aspects such as shock formations and the base pressure problem (see [1] and [2]). The investigations were extended to aerothermal topics like heat transfer measurements [3] and trailing edge cooling [4]. With the advent of numerical methods single blade row calculations were conducted to match the experimental data ([5], [6] and [7]) whereas later computations simulated the steady flow through multiple rows ([8] and [9]). Recent investigations in the VKI CT3 blow-down facility [10] focused on very accurate and transient heat transfer measurements at engine representative Mach and Reynolds numbers, with partial simulation of cooling flows (VKI stator), but no inclusion of secondary flows (see [11] and [12]).

Another well documented and long-term measurement campaign in a high-speed environment has been established and conducted in the blow-down type facility at QinetiQ (cf. [13] and [14]). In close collaboration with the University of Oxford, the uncooled MT1 HPT stage geometry was tested at total to total pressure ratios below three, in the recent past focusing on aspects of inlet temperature and swirl variations onto surface temperature, heat transfer and performance [15]. Whereas the obtained Reynolds numbers are engine representative, the Mach number levels at stator and blade exit reach high subsonic values. Compared to the activities at VKI and QinetiQ, the HWSS campaign focuses on very accurate performance measurements in an engine representative environment with full modeling of cooling and secondary flows at pressure ratios beyond 4.

Apart from academic research, engine manufacturers have been investigating this topic for many decades. Pratt & Whitney [16] developed and tested uncooled high-work transonic turbines with different reactions for the E^3 demonstrator engine, aiming at a target efficiency of 90.3% at pressure ratios slightly larger than 4. An additional research topic was the impact of rotor tip clearance on loss at a pressure ratio of 3.9. The work comprises a comparison of uncooled unshrouded and partially shrouded blades at different tip gaps (see [17]).

MTU designed a high-work turbine for a small helicopter engine working at a pressure ratio of 3.6 [18]. The development program was similar to the HWSS program, including preceding cascade experiments, a thorough investigation of stator/rotor matching, film cooling and rotor tip clearance effects. Compared to the engine research at P&W and MTU the HWSS turbine runs at a higher pressure ratio (between 4 and 4.5) and features full cooling and leakage flows.

Investigations of the unsteady interaction of transonic stages started in parallel at Oxford University and at MIT (see [19], [20] and [21]) and were accompanied by the emerging unsteady numerical flow solvers (see [22]-[24]). Since then this topic has been of continuous interest of both academic and industrial research (cf. [25], [26] and [27], the latter achieving pressure ratios of 4).

The common understanding of the requirements for an efficient supersonic turbine can be summed up as follows. In a blade context shock losses, wake thickness and flow separation need to be minimised. In a stage context flow unsteadiness and the amount of wake/shock crossings should be reduced. More specifically, a smaller angle between shocks and wakes leads to a smaller loss increase during the multiple shock crossings. In order to investigate the potential of a transonic HPT, a high-speed turbine rig called HWSS (High-Work Single-Stage) was installed at DLR Göttingen and investigated both experimentally and numerically. This research work was done within the German government funded LuFo-3 programme. This paper focuses on the first of two builds, featuring a single-stage HPT (hence referred to as Build-1) whereas the second build is an extension to a 1.5-stage HPT. Hence this paper does not cover HP/LP interaction. After a short introduction of the transonic aerofoil design philosophy and a summary of preceding cascade tests the HWSS design and test results will be described in detail.

DESIGN

A feasible aerodynamic concept for a high-pressure turbine with supersonic exit conditions needs, in particular, to address the following issues:

1. Moderate exit losses of the stator vane at part-power (off-design) conditions in order to allow for a smooth ramp-up of the HP-turbine power in the start-up phase of the engine
2. Minimum shock-losses at design point for overall competitive row and component efficiencies
3. High flow turning of the rotor blade for high work
4. Suitable aerodynamic inlet conditions to the downstream blade row

In the context of aerofoil designs for establishing supersonic aerodynamics for both stator and rotor, these four main requirements translate into:

1. No allowance for flow separation on the stator for any exit Mach number
2. Minimum un-covered turning of the flow in the blade row and proper matching of trailing edge blockage to exit area for the exit Mach number at design point
3. Fast acceleration to supersonic Mach numbers and rapid flow turning followed by an expansion to the design Mach number with minimum turning
4. Minimise the strength of the trailing edge shock system

The high flow turning delivering the high rotor work automatically leads to small angles between the trailing edge shocks and the downstream blade row. In addition, favourable inlet conditions for an LP stage are obtained by preventing flow separation and weakening the trailing edge shock system. Following these basic principles, a number of designs were evaluated for cascade tests in the high-speed cascade facility at DLR Göttingen. Experimental and numerical investigations were conducted for a stator and a rotor aerofoil for a broad range of Mach numbers including the effect of film-cooling. Especially for the rotor simulations the numerical results showed a relatively flat loss characteristic with a loss minimum at the respective design point with an isentropic exit Mach number Ma_{is}=1.25. In terms of loss coefficient the agreement with measurements was only satisfying in the subsonic region. Recently the reason for the deviations has been identified as a malfunction of the flow dryer in the experiment. For a detailed presentation of the results see [28]. Apart from the efficiency, results of flow angles and pressure distributions compared very well, such that the knowledge gathered in the course of the cascade investigations encouraged the design of a rotating rig experiment.

This paper focuses on the first out of two builds, consisting of a single-stage, shroudless high-pressure turbine, designed to work at pressure ratios between PR=4 and 4.5. The blade rows consist of 30 stator and 60 rotor blades, thus allowing a convenient stator/rotor count ratio for unsteady numerical simulations. Extensive 3D studies have been conducted, examining the influence of rotor chord length, hub radius and passage expansion ratio on the aerodynamic performance. The resulting annulus shape is a compromise between aerodynamic efficiency and allowable stresses. Aerofoils for both blade rows were designed based on the experience gathered during the cascade experiments. The design Mach numbers for stator and rotor are Ma_{is}=1.1 and 1.25, respectively. In contrast to the previous investigations the aerofoil shapes were adapted to the radially changing Mach number, ensuring that each blade section is working at its aerodynamic optimum. Despite the targeted operating conditions the aerodynamic design is not purely driven towards supersonic speeds but rather a weighted blend of both good subsonic and high-speed performance.

The in-house numerical software package Hydra as well as the commercial flow solver suite by Numeca were used to quantify the sensitivity of the HPT to the imposed pressure ratio as well as the rotational speed. The results show a favourable variation of efficiency with a slow degradation of performance for a broad speed range and a significant drop of performance below 80% nominal speed. In addition, the influence of deviations introduced, e.g., during manufacturing or operational wear has been investigated and exchange rates for efficiency and capacity derived. Again, no significant drop of aerodynamic properties due to external deviations was observed. Prior to the rig tests additional numerical analysis of the time-dependent flow at operating conditions was conducted. Both local results such as flow angle as well as global quantities like efficiency agree well with results from steady analysis.

Apart from the annulus and blade design, considerable effort was put on the design of the rotor front rim seal. Based on a conventional design, the shingling geometry was altered such that recirculation close to the entry to the main passage as well as mixing losses are reduced. The new design has a reduced gap width and thus stronger acceleration of the leakage air, which leads to better mixing and at the same time smaller deviations of the flow angle from the design conditions near the hub surface, yielding a noticeable overall efficiency benefit. The HWSS annulus and the rotor front cavity are shown in Figure 2.

Due to the high rotational speed of the HWSS the rotor tip geometry is a relatively simple double-sided squealer design.

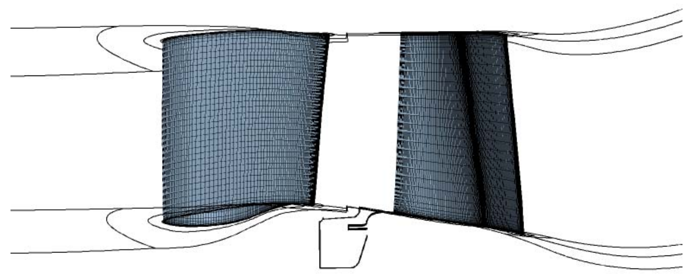

Figure 2: HWSS annulus and rotor front cavity

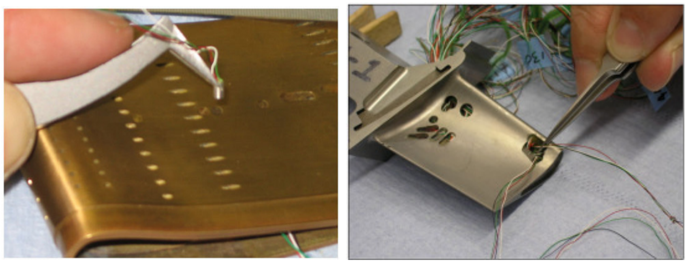

Figure 3: Assembly of instrumented blades

For a tip gap width of 1% blade height, a study of the influence of the squealer depth on the stage efficiency lead to a squealer depth of approximately 2.5% of blade span. Two tip clearances were investigated. At design speed the large clearance is 2% and the small clearance is 1% of the blade height.

In order to closely resemble engine conditions and thus enable a direct transfer of rig results to engine applications, both blade rows were equipped with representative cooling films and two tip holes in the squealer bottom. In addition, realistic rotor front and rear leakage flows are part of the experimental setup.

INSTRUMENTATION & MEASUREMENT PROGRAM

An extensive measurement program was specified, including boundary layer measurements at the HP inlet as well as rakes and multi-hole probes for measuring time-dependent radial distributions of pressure and temperature at several planes in the test section. Additional pressure transducers in the annulus were used to monitor the circumferential periodicity. The tip clearance was measured throughout the whole measurement program and found to be very close to the specified value. Stator and rotor were delicately equipped with Kulite pressure transducers (see Figure 3) which -in the case of the rotor by means of a telemetry- monitored time-dependent pressure distributions at 15%, 50% and 90% blade height. The whole blade instrumentation comprises 90 pressure transducers (some of them redundant), 18 strain gauges and three thermal

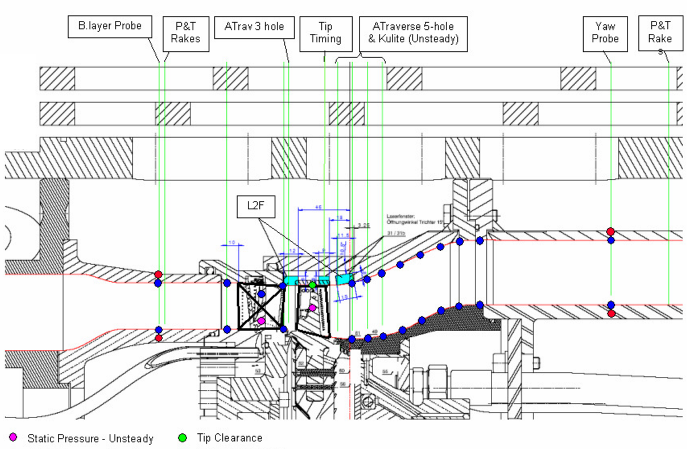

Figure 4: Instrumentation of the HWSS rig

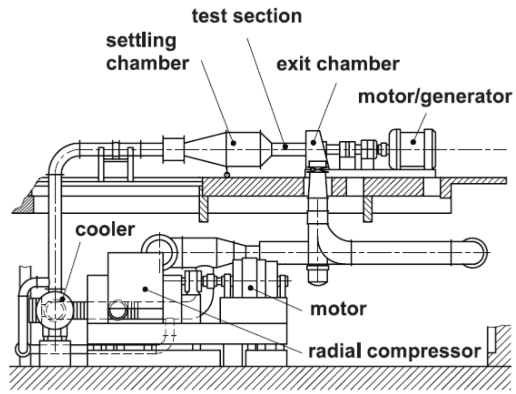

Figure 5: Sketch of the wind-tunnel RGG

sensors, resulting in a highly complex set-up. The instrumentation of the test section is shown in Figure 4.

While the aerodynamic design and instrumentation of the blades was done at RRD, the design of the test section, manufacturing of all parts and the testing program were carried out at DLR Göttingen. The HWSS HPT was installed in the wind-tunnel RGG shown in Figure 5. The facility is a closed-loop wind-tunnel, equipped with a 4-stage radial compressor and capable of inlet temperatures between 295K and 450K and compressor delivery pressure ratios up to 6. However, the maximum allowable pressure ratio for the HWSS runs was limited to 4.5. Also, the maximum rotational speed of 14,500 rpm was reduced to 11,000 rpm in the experiments. Turbine power was picked up by a 1200kW motor, acting as a generator and fed back into the grid. Data for power measurements was provided by a shaft encoder and a torque meter, yielding a torque measurement accuracy of ≈0.15%. The mass flow in the main passage was determined redundantly, using a calibrated Venturi nozzle and static pressure tappings in the HP inlet. The remaining flows such as film coolant and leakage air were measured with orifice plates. Prior to the tests, the NGV throat area was measured and found to be in very good agreement with the specification.

The test program was split into performance and traverse measurements. Performance was measured within a range of 30-110% nominal speed and between 10-100% nominal power for two different tip clearances. According to standard Rolls-Royce naming conventions, the following relations are used for non-dimensionalization:

$$\mathrm{NHRT} = N/\sqrt{T_{41}} \quad \text{(reduced speed)} \tag{1}$$

$$\mathrm{WRTP} = \mathrm{w}_{41}\sqrt{\mathrm{T}_{41}}/\mathrm{p}_{40} \quad \text{(capacity)} \tag{2}$$

$$\mathrm{DHT} = P_r/w_{41}/T_{41} \quad \text{(rotor specific work)} \tag{3}$$

where 41 denotes the stator exit plane. The isentropic efficiency is defined as

$$\eta = P_r/P_{ideal} \tag{4}$$

with P_r measured by the torque meter. The ideal work is calculated using an isentropic relation

$$P_{ideal} = w \int_{T_{44is}}^{T_{41}} c_p(T) dT \qquad (5)$$

with T_{44is} obtained assuming isentropic expansion across the stage

$$\int_{T_{41}}^{T_{44is}} \frac{c_p(T)}{T} dT = R \ln\left(\frac{p_{44}}{p_{40}}\right) \qquad (6)$$

NUMERICAL SIMULATION

A dedicated numerical model was set up for validation purposes. The analysis was conducted with the CFD package by Numeca [29] consisting of the mesh generator Autogrid v7.2 and the solver FineTurbo v7.2. The Navier-Stokes equations are resolved using a block-structured, co-located finite volume method. The diffusive terms are calculated by means of a second-order central approximation. For the convective, term a Jameson-type second-order central approximation scheme with scalar dissipation [30] is used. Accuracy can be increased by using a reconstruction procedure with the gradient computed following a least-square approach. Steady solutions are obtained via a fourth-order Runge-Kutta method with local time-stepping. The iterative process is accelerated using multigrid and residual smoothing. Steady simulations are based on a mixing-plane approach with the interface placed downstream of the stator but upstream of the rotor seal cavity, hence a proper interaction of the rotor potential field and leakage air is ensured. Time-dependent simulations were conducted using a sliding plane at the same position as in the steady runs. The number of time steps per vane passage was chosen to be 50, ensuring a full convergence of the residual within each time step. Film cooling was imposed using a source-term approach. Each cooling hole spreads over a sufficient number of surface patches, such that exit momentum is close to a fully-meshed cooling hole. Note that the numerical model uses just one tip hole. The flow field is assumed to be fully turbulent and simulated with the Spalart-Allmaras turbulence model [31]. Gas temperature in the range of 250-400K allowed the model to treat air as a perfect gas.

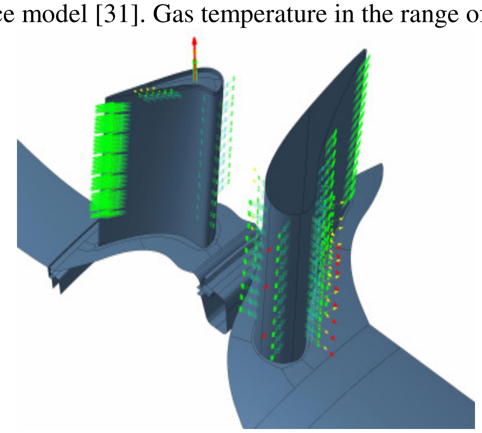

Figure 6: Computational domain with film cooling source terms (distorted view)

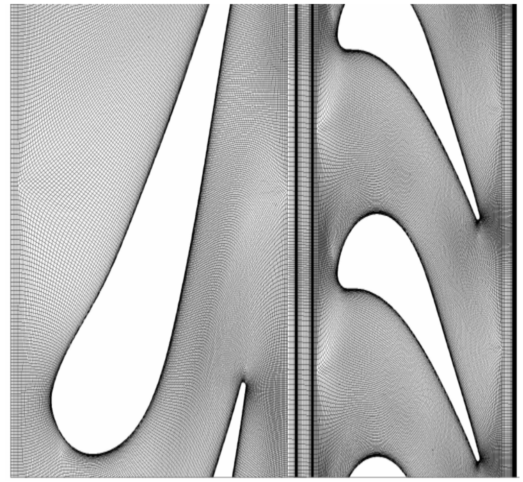

Figure 7: Blade to blade mesh (fine grid, distorted view)

A structured multi-block mesh was created for the Build-1 geometry. Apart from the tip gap block, the whole grid is conformal. The geometrical deviations to the actual geometry are a missing hub fillet in the rotor as well as a slightly smaller tip gap. The latter was corrected using exchange rates provided by the measurements and numerical analysis prior to the tests. The mesh consists of 16 million points on the finest grid level and 2 million points after one coarsening step. y^+ values of 0.2 (fine) and 1 (coarse) indicate that boundary layers are well resolved on both grids. The coarse grid was used for unsteady analysis and the evaluation of speed-lines whereas the fine grid was utilized for steady, in-depth analysis and individual verification of results obtained on the coarse grid. The computational domain with the imposed cooling flows is shown in Figure 6, whereas Figure 7 gives an indication of the very high spatial resolution of the domain, capable of capturing the shock structure accurately.

RESULTS

Performance

One of the design intents of the HWSS was to choke the flow through the stator in the operating point, thus ensuring a stable inflow for the down-stream rotor throughout the flight envelope. A convenient check whether the stator in the rig test chokes is to overlay the isentropic Mach number distributions, calculated from surface pressure measurements in the stator for the two investigated tip clearances. Figure 8 shows that at the design point the upstream effect is bounded by the stator trailing edge shock, hence the mass flow through the throat area remains constant. Measuring the tip clearance over the whole range of speed and rotor specific work also revealed that the tip gap is not only a function of the rotational speed but of the extracted work, too. Using the example of the smaller tip clearance, Figure 9 shows that for a given speed an increase of

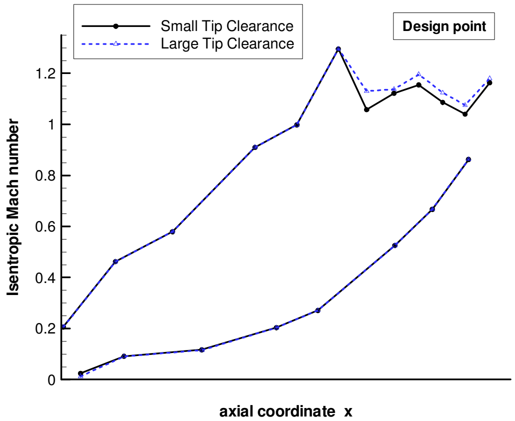

Figure 8: Influence of rotor tip clearance on stator flow

rotor work can lead to a clearance reduction of almost 20% of the whole range, which results from a lower casing temperature at higher specific work. Corrections have been applied before comparing measured efficiencies with numerical results. The variation of efficiency as a function of speed and work is shown in Figure 10. Compared to the numerical simulation, the measured work in the experiments contains a few components not reflected in the numerical model such as the rotor work on leakage air (pumping) and rotor disk friction. The measured and predicted efficiency for 100% nominal speed is shown in Figure 11. The different off-design behaviour towards low specific work in the steady simulation is not surprising. Note that these are results from steady simulations on the coarse grid. The agreement could be improved by switching to the finer grid but even more by taking unsteady effects into account, e.g. by using the non-linear harmonic method in FineTurbo. For higher rotor work the agreement is very good, with the measured value scatter following the predicted distribution. At design conditions an additional simulation was done on the fine grid, yielding a slightly higher efficiency which is still within the

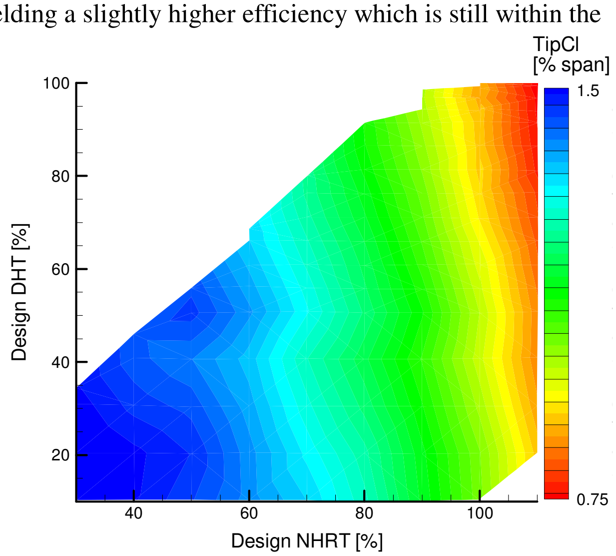

Figure 9: Effect of NHRT and DHT on small rotor tip clearance

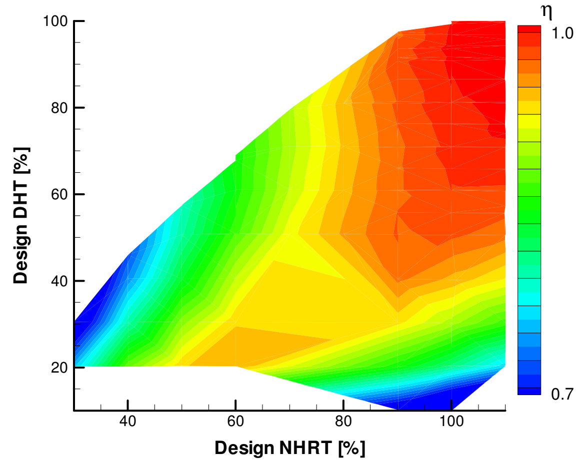

Figure 10: Efficiency distribution for large tip clearance

uncertainty range of the experiments. For future comparisons (Build-2) the numerical setup should be closer to the rig (fillet, tip hole) whereas on the experimental side the uncertainties regarding pumping, etc. should be clarified. Then an even better agreement is expected.

According to Figure 12 the numerical model constantly underpredicts the measured capacity. Changing to the finer mesh, the difference is reduced by 50%. It is expected that a comparison of the throat areas in the rig and in the computational domain will yield slight differences. Overall, the prediction accuracy obtained in this capacity comparison is

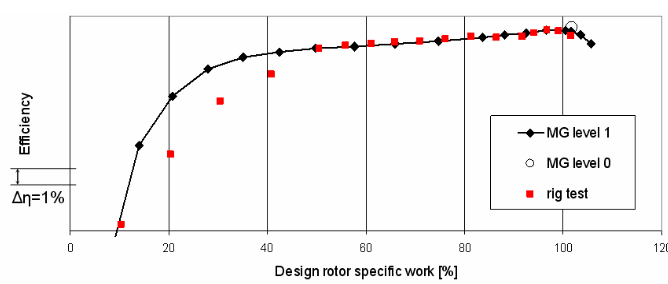

Figure 11: Comparison of measured and predicted efficiency at 100% speed

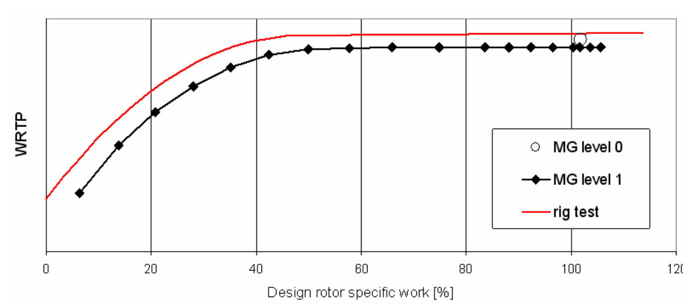

Figure 12: Comparison of measured and predicted capacity at 100% speed

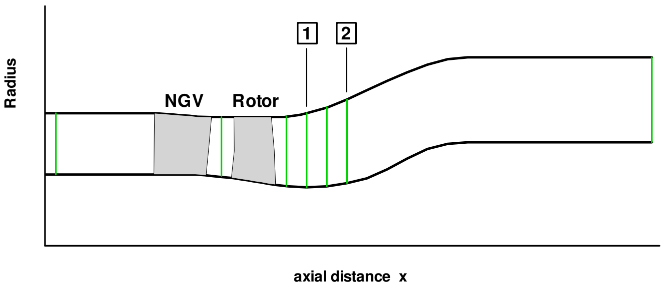

Figure 13: Probe measurement planes

within the expectations and deemed satisfactory. Further findings of the performance measurements are that the stator chokes for >48% design rotor specific work whereas the limit for the rotor is reached at 84% design DHT. Peak efficiency was obtained at 110% design speed.

Area traverses

During the area traverse measurements, three steady probes and one unsteady (Kulite) probe were simultaneously installed at defined axial and circumferential positions. By radial movement of the probes and circumferential movement of the NGV the flow values could be determined over 1.3 pitches of the NGV and at radii from slightly above the hub to the casing. The axial positions of the measurement planes are shown in Figure 13. In the inlet duct upstream of the stator, flattened Pitot probes especially adapted for the endwall boundary layer measurements were used. The probe used between stator and rotor was especially adapted for transonic flow and yields circumferential (yaw) angle, Mach number and total temperature and pressure. For steady flow measurements,

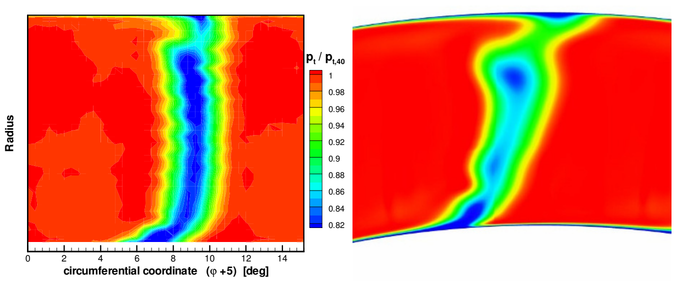

Figure 14: Total pressure ratio distribution in stator exit at design point (left: exp., right: CFD)

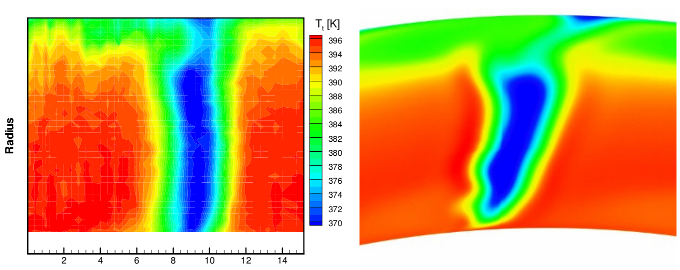

Figure 15: Total temperature distribution in stator exit at design point (left: exp., right: CFD)

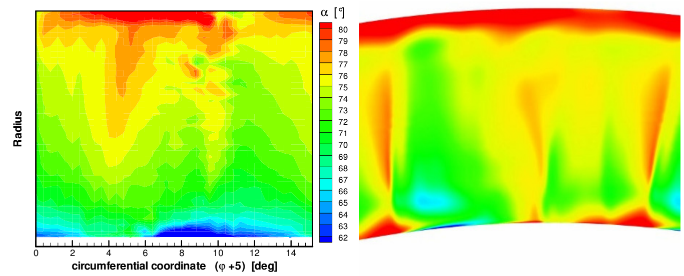

Figure 16: Flow angle distribution in stator exit at design point (left: exp., right: CFD)

probes were automatically turned into the flow direction and data recorded at zero probe incidence. To measure the unsteady flow downstream of the rotor a single sensor (Kulite) unsteady probe was installed. The instantaneous pressure signal from the Kulite sensor was sampled at 500kHz from which 20,000 points were recorded. This means that 7 to 9 revolutions of the rotor were stored. The unsteady time trace was subsequently ensemble-averaged over 4 revolutions to get two pitches of the rotor at a specified probe circumferential angle. In order to determine the ensemble-averaged Mach number, yaw angle and total pressure from such a single sensor probe, measurements for at least three probe incidence angles have to be performed. The following comparison of stator and rotor traverses uses numerical results from steady runs on the fine grid. Along the measurement plane between stator and rotor Figure 14 and Figure 15 show a very good agreement for the distributions of the total pressure ratio and total temperature both with the main difference being a slightly more pronounced horseshoe vortex near the casing in the experiments. Regarding the flow angle distribution in Figure 16 a good quantitative agreement is observed but the flow structure is not as easily identified as in the total quantities. Notable differences exist close to the hub surface, probably resulting from the position of the mixing plane near the region where leakage flow interacts with the main flow. Again, the departure from the mixing plane approach and inclusion of unsteady effects is expected to yield a better agreement.

A similar comparison is done for Kulite measurements obtained for the large tip clearance in the rotor exit at an axial distance to the trailing edge of approximately one chord length (plane “1” in Figure 13). Both the total pressure ratio in Figure 17 and flow angle in Figure 18 show a stronger tip vortex in the

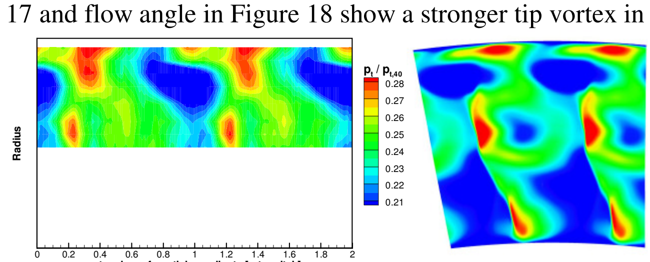

Figure 17: Total pressure ratio distribution in rotor exit at design point (left: exp., right: CFD)

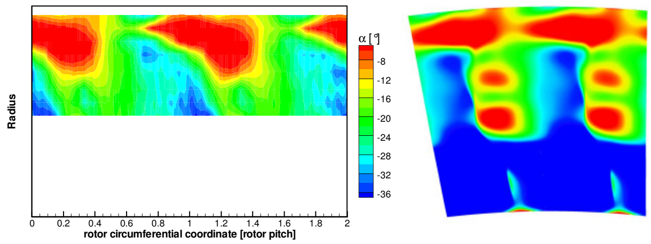

Figure 18: Flow angle distribution in rotor exit at design point (left: exp., right: CFD)

experiments, which could be the result of more coolant air injected through two tip holes compared to the single dust hole in the numerical model. Another reason could be that the predicted flow is overall slightly too low, which is indicated by Figure 12. Additional comparisons were done at a second measurement plane (plane “2” in Figure 13) where flow quantities have undergone further mixing. Figure 19 shows radial distributions of total pressure ratio, Mach number, circumferential and radial flow angles obtained from measurements at two different tip clearances and the numerical result. The tip gap in the computational model was close to the large tip clearance in the experiments. The agreement is very good in terms of pressure ratio whereas the predicted flow is more axial at a slightly lower Mach number level. Again, less

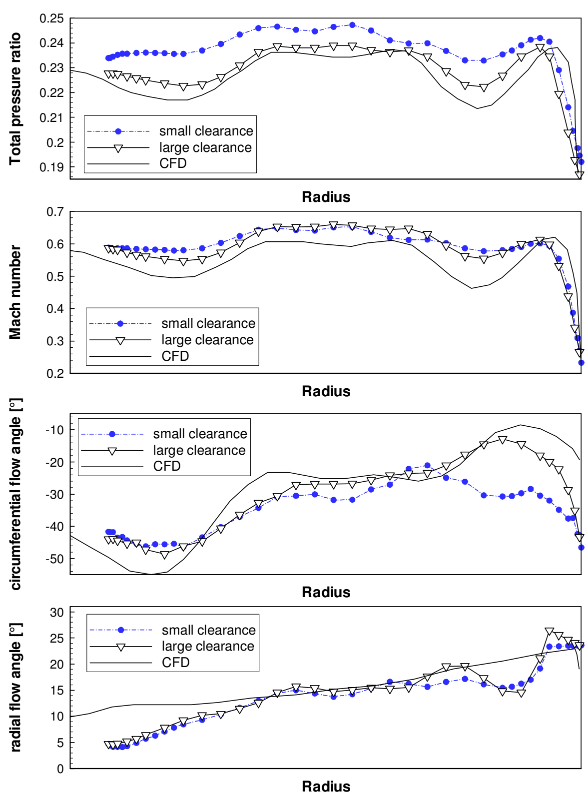

Figure 19: Circumferentially averaged distribution of total pressure ratio, Mach number, circumferential and radial angle downstream of the rotor (x=28mm)

cooling from the tip region in the simulations leads to smaller regions dominated by secondary flow. However, as mentioned above, the flow in the simulation could be slightly too low. The calculated radial flow angles show less variation than in the experiment while matching the overall level quite well.

Unsteady data

In addition to the steady calculations of the HWSS flow field, an unsteady simulation was done using the sliding plane approach on the coarse grid. Time-dependent pressure plots were calculated from the data recorded by the pressure transducers on the stator and rotor. As a number of Kulites were damaged throughout the test program, relatively complete data sets are only available for the early runs. From this data pool a test run with similar boundary conditions as in the simulation was chosen. Note that the inlet pressure in the experiment is slightly slower than in the simulation. Pressure signals were extracted from the numerical result at the positions of the Kulite pressure transducers and compared with the measurements. In contrast to the second build, no trigger signal was available in the Build-1 campaign, hence the recorded data cannot be associated with the rotor position relative to the stator. Therefore, the compensation of the phase difference between measurement and simulation had to be done manually.

For the comparison, only pressure signals without excessive noise are selected. The range of prediction accuracy shown in the following figures is representative of the pool of available measurements. For the stator only one transducer position at mid-span was chosen (marked in Figure 20) whereas more results will be shown for the rotor. See Figure 20 for the naming convention.

Starting with the stator, the static pressure signals recorded and calculated at the late suction side at mid-span reproduce the rotor passing frequency of 9600Hz (see Figure 21). Especially in the numerical solution for each blade passing a distinct double pressure peak is observed, which is probably connected with unsteady shock movement. The lower mean pressure in the experiment is at least partially caused by the difference in inlet conditions. Looking at the hub region of the rotor a very good

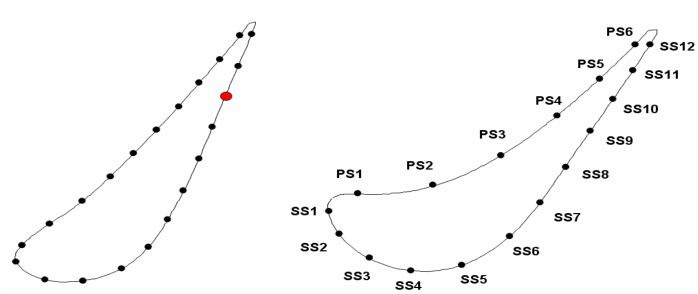

Figure 20: Position of Kulite pressure transducers on stator (left) and rotor (right), distorted view

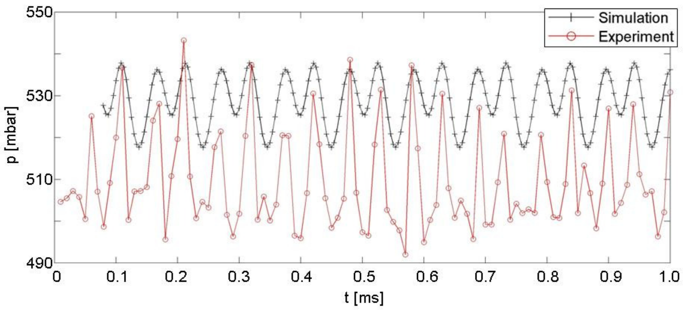

Figure 21: Comparison of stator pressure signals, 50% span

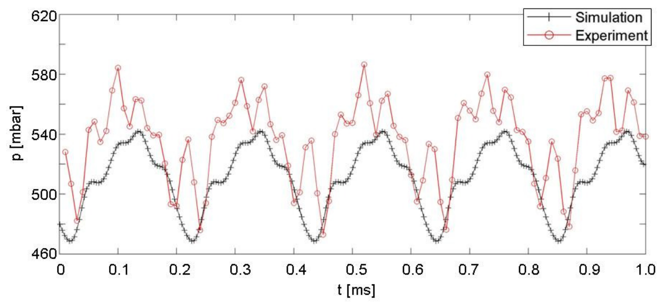

Figure 22: Comparison of rotor pressure signals, PS2 at 15% span

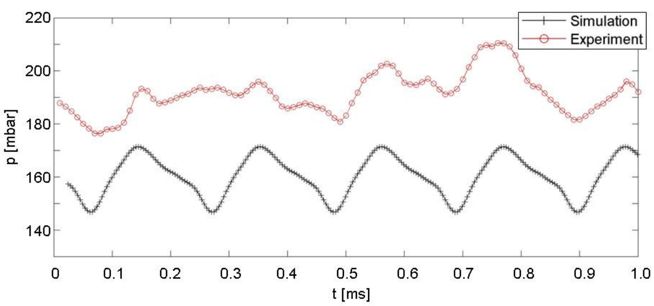

Figure 23: Comparison of rotor pressure signals, SS12 at 15% span

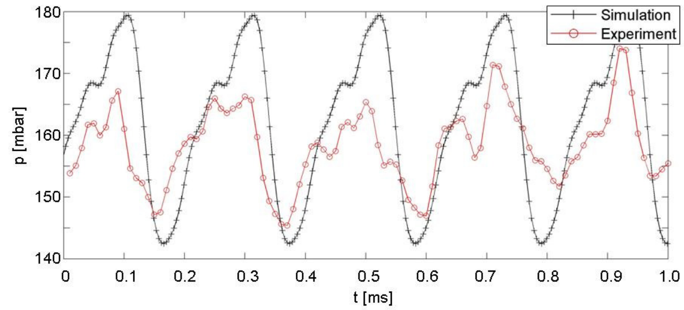

Figure 24: Comparison of rotor pressure signals, SS12 at 50% span

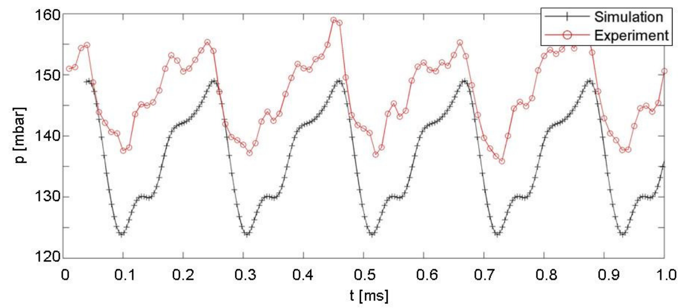

Figure 25: Comparison of rotor pressure signals, SS9 at 50% span

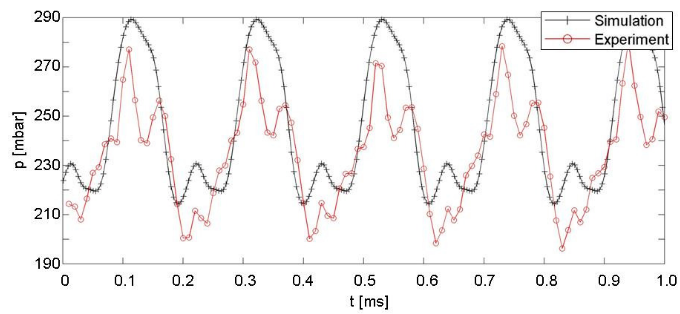

Figure 26: Comparison of rotor pressure signals, SS5 at 50% span

agreement is obtained for the early pressure side (see Figure 22). Again, the stator passing frequency of 4800Hz is well resolved. An interesting difference compared to the simulation is a pronounced local pressure peak while at the same time the flow solver calculates a pressure minimum. A different behavior is observed on the suction side close to the trailing edge in Figure 23. While the pressure variations agree well, the flow solver yields approximately 30mbar lower pressure fluctuations. A similar behavior, i.e., an underprediction of the pressure in the hub region was already observed in the comparison of the circumferentially averaged distributions in Figure 19. Continuing the comparison close to the trailing edge but moving radially outwards to the midsection, the agreement improves significantly (cf. Figure 24) whereas a small offset returns while moving towards the leading edge in the following two figures. It should be noted again, that not all uncertainties, in particular, regarding the boundary conditions of the leakage air could be ruled out. As the pressure difference of 5-10mbar is small, the conclusion is drawn that most of the important unsteady flow features are captured.

CONCLUSION

A modern, highly-loaded single-stage HPT was designed at Rolls-Royce Deutschland and manufactured, assembled and tested at DLR Göttingen. Heavy use of numerical methods during the design phase helped to optimize the annulus, blade geometry and shingling as well as to quantify the influence of tip gap width and squealer geometry. An extensive measurement programme was specified, that apart from performance and traverse measurements also yielded pressures, temperatures and stresses on the blade surfaces of both rows. The performance results show a favourable characteristic with good efficiency over a broad working range with the targeted peak value close to the operating point, which is in line with the expectations. A thorough comparison with numerical results yields a good agreement of efficiency distributions and area traverses as well. Most of the visible differences are caused by restrictions to steady modelling approaches and uncertainties regarding some of the boundary conditions. A comparison of unsteady pressure signals on the blade surfaces demonstrates that numerical methods are capable of capturing most of the flow features reliably. Recommendations for the analysis of the successor build were derived from comparisons between the Build 1 data and CFD model.

ACKNOWLEDGMENTS

This work was carried out within the German government funded research project LuFo-3 "*Transonic Single-Stage High-Pressure Turbine"* under the reference number 20T0301A. The support is gratefully acknowledged.

REFERENCES

[1] Sieverding, C. H., "Experimental Data on Two Transonic Turbine Blade Sections and Comparison with Various Theoretical Methods", VKI LS 59, Transonic Flows in Turbomachinery, 1973

[2] Sieverding, C. H., Stanislas, M., Snoech, J., "The Base Pressure Problem in Transonic Cascade", ASME 79-GT-120, 1979

[3] Arts, T., Heider, R., "Aerodynamic and Thermal Performance of a Three-Dimensional Annular Transonic Nozzle Guide Vane, Part 1: Experimental Investigation", AIAA 94-2929, 1994

[4] Sieverding, C. H., Arts, T., Denos, R., Martelli, F., "Investigation of the Flow Field Downstream of a Turbine Trailing Edge Cooled Nozzle Guide Vane", ASME 94-GT-209, 1994

[5] Arnone, A., Stecco, S. S., "Transonic Cascade Flow Prediction using the Navier-Stokes equations", ASME 91-GT-313, 1991

[6] Turner, M. G., Liang, T., Beauchamp, P. P., Jennions, I. K., "The Use of Orthogonal Grids in Turbine CFD Computations", ASME 93-GT-38, 1993

[7] Heider, R., Arts, T., "Aerodynamic and Thermal Performance of a Three-Dimensional Annular Transonic Nozzle Guide Vane, Part 2: Assessment of a Three-Dimensional Navier-Stokes Solver", AIAA 94-2930, 1994

[8] Dawes, W. N., "Multi-Blade Row Navier-Stokes Simulations of Fan-Bypass Configurations", ASME 91-GT-148, 1991

[9] Adamczyk, J. J., Celestina, M. L., Beach, T. A., Barnett, M., "Simulations of Three-Dimensional Viscous Flow Within a Multistage Turbine", ASME 89-GT-152, 1989

[10] Sieverding, C.H., Arts, T., "The VKI Compression Tube Annular Cascade Facility", ASME Paper, 92-GT-336, 1992

[11] Didier, F., Dénos, R., Arts, T., 2002, "Unsteady rotor heat transfer in a transonic Turbine Stage," ASME Paper GT-2002-30195, 2002

[12] Iliopoulou, V., Dénos, R., Billiard, N., Arts, T., "Time - Averaged and Time-Resolved Heat Flux Measurements on a Turbine Stator Blade using Two-Layered Thin-Film Gauges", ASME Paper GT2004-53437, 2004

[13] Chana, K.S., Jones, T.V., "An Investigation on Turbine Tip and Shroud Heat Transfer", J. Turbomach., 125, no. 3, pp. 513-520, 2003

[14] Povey, T., Chana, K.S., Jones, T.V., Hurrion, J., "The effect of Hot-Streak on HP Vane Surface and Endwall Heat Transfer: an Experimental and Numerical Study", ASME J. Turbomach., 129, pp. 32-43, 2007

[15] Qureshi, I., Smith, A. D., Chana, K. S., Povey, T., "Effect of Temperature Nonuniformity on Heat Transfer in an Unshrouded Transonic HP Turbine: An Experimental and Computational Investigation", ASME Paper GT2010-22700, 2010

[16] Crow, D. E., Vanco, M. R., Welna, H., Singer, I. D., "Results from Tests on a High Work Transonic Turbine for an Engergy Efficient Engine", ASME 80-GT-146, 1980

[17] Patel, K. V., "Research on a High Work Axial Gas Generator Turbine", SAE 800618, 1980

[18] Dietrichs, H.-J., Malzacher, F., Broichhausen, K., "Development of a HP-Turbine for a Small Helicopter Engine", AGARD Conference on Technology Requirements for Small Gas Turbines , Conference Proceedings, No. 537, Montreal, CDN, 1993

[19] Johnson, A. B., Oldfield, M. L. G., Rigby, M. J., Giles, M. B., "Nozzle Guide Vane Shock Wave Propagation

and Bifurcation in a Transonic Turbine Rotor", ASME 90-GT-310, 1990

[20] Guenette, G. R., Epstein, A. H., Giles, M. B., Haimes, R., Norton, R. G. J., "Fully Scaled Transonic Turbine Rotor Heat Transfer Measurements", ASME 88-GT-171, 1988

[21] Abhari, R. S., Guenette, G. R., Epstein, A. H., Giles, M. B., „Comparison of Time-Resolved Turbine Rotor Blade Heat Transfer Measurements and Numerical Calculations", ASME 91-GT-268, 1991

[22] Rai, M. M., "Navier-Stokes Simulations of Rotor-Stator Interaction Using Patched and Overlaid Grids", AIAA Journal of Propulsion and Power, Vol. 3, pp. 387-396, 1987

[23] Giles, M. B., "Stator/Rotor Interaction in a Transonic Turbine", AIAA Journal of Propulsion, Vol. 6, p. 621, 1990

[24] Chen, J. P., Celestina, M. L., Adamczyk, J. J., "A New Procedure for Simulating Unsteady Flows Through Turbomachinery Blade Passages", ASME 94-GT-151, 1994

[25] Jennions, I. K., Adamczyk, J. J., "Evaluation of the Interaction Losses in a Transonic Turbine HP Rotor/LP Vane Configuration", ASME 95-GT-299, 1995

[26] Yao, J., Carson, S., "HPT/LPT Interaction and Flow Management in the Inter-Turbine Space of a Modern Axial Flow Turbine", ASME GT-2006-90636, 2006

[27] Tanimitsu, H., Nakamata, C., Fujimoto, S., Aoki, Y., Ishizaki, M., "Development of Simple and High-Performance Technology for Turbine", IHI Engineering Review, Vol. 41, No. 1, 2008

[28] Wolf, T., Kost, F., Janke, E., Haselbach, F., Willer, L. "Experimental and numerical studies on highly loaded supersonic axial turbine cascades", ASME Turbo Expo GT2010-23808

[29] http://www.numeca.com

[30] Jameson, A., Schmidt, W., Turkel, E., "Numerical solutions of the Euler equations by finite-volume methods with Runge-Kutta time stepping schemes", AIAA Paper 81-1259, 1981

[31] Spalart, P.R., Allmaras, S.R., "A one-equation turbulence model for aerodynamic flows", AIAA Paper 92-439, 1992

